Design and experimental research of angle self-compensation setup for BSDF measurement

Chao Qi (齐 超)*, Hongchen Liu (刘洪臣), Yuanli Wei (韦袁丽), and Jingmin Dai (戴景民)

School of Electrical Engineering and Automation, Harbin Institute of Technology, Harbin 150001, China

**E-mail: qichao@hit.edu.cn*

Received July 11, 2008

When using a single reference to measure the bi-directional scattering distribution function (BSDF), the incident zenith angle of the tested sample must be identical to that of the reference. In order to get the hemisphere space scattering characteristic on the sample surface, usually a motor drives the sample tilting, then the incident zenith angle is changed and needs to be the compensated by another motor. We mathematically deduce the expression of compensation angle when the incident zenith angle is changed by the rotation of motor. After the incident angle is compensated, the scattering zenith angle and azimuth angle are deduced too. The uncertainty of the system is 0.75%. Scattering measurements are performed on copper sample with visible light under different temperatures.

OCIS codes: 120.5820, 220.4830, 070.4560.

doi: 10.3788/COL20090705.0403.

Most objects have anisotropic reflectance, which can be described by the bi-directional scattering distribution function (BSDF). It is very important to obtain high quality bi-directional scattering data sets for BSDF research and applications. Those data sets may be used to validate the present various bi-directional reflectance/transmittance distribution function (BRDF/BTDF) models and retrieve the surface characteristics of the objects in remote sensing applications[1,2]. According to Ref. [3], the BSDF is a ratio of the scattering radiance to the incident irradiance. It mostly depends on four angles (two for the incident radiation and two for the scattering radiation) and is a function of the wavelength, surface roughness, material properties, and temperature. The characteristics of spatial light scattering from material surface can be effectively described by BSDF, so BSDF is generally applied in several fields, such as national defense, military affairs, soil resource remote sensing, vegetation monitoring, environment and climate monitoring, stray light suppression, etc.[4−9].

There are two ways to obtain the entire zenith angle and azimuth angle which are covered by light on the sample. The first is to mount the light source on a movable arm or to use a turning mirror on a movable arm, and to use a detector to measure the distribution of scattering light by moving it around the entire hemisphere. To measure the full BSDF, this process must be repeated many times, moving the light source again and again to measure different incident angles. So this method has been discarded. The second is to fix the light source and to move the sample or its roll and yaw axes, so that the scattering light goes into the constrained detector which can only move in one plane.

Based on the second method described above, we designed the angle self-compensation setup with three degrees of freedom for scattering measurement, as shown in Fig. 1. The crankshaft of the No. 1 motor is parallel to the table-board and perpendicular to the normal of the sample plane. This mototr drives the sample running within the range from $-180°$ to $+180°$. At the same time, the crankshaft of the No. 2 motor intersects that of the No.1 motor at the center of the sample, plumbs in the bottom, and drives the No. 1 motor and the sample rotating together. It is obvious that the direction of the No. 1 motor crankshaft is variable in the space plane during the process of running. In addition, the scope that the No. 2 motor drives the sample turntable running is also from $-180°$ to $+180°$, and the angles of sloping running and rotating are indicated by dial 1 and dial 2, respectively. The combination of the No. 1 and the No. 2 motors can implement the changes of and the incident zenith angle $\theta_{\rm i}$ and the azimuth angle $\varphi_{\rm i}$. The No. 3 motor crankshaft is parallel to that of No. 2, which drives the detector arm rotating around the turntable axis within the range from $-180°$ to $+180°$ via a decelerating gear. A detector is located on an adjustable bracket in the hopper chute of the detector arm, and the distance from the detector to the sample can be adjusted, so the scattering radiance which comes from the sample can be measured as the function of space scattering angle $(\theta_{\rm S}, \varphi_{\rm S})$. The control of the sample direction and the acquisition of the measured data are completed by the computer automatically, therefore we can study the space scattering property and spectral characteristic of the objective material.

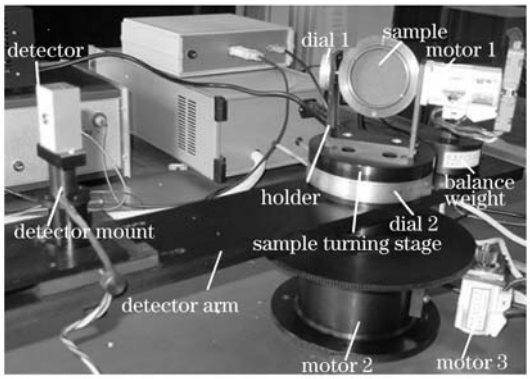

Fig. 1. BSDF measurement setup.

The closed-loop control of pulse negative feedback response motor displacement is prevalently used in system software, so that we can achieve more accurate position control and more stable speed of motor rotation, as shown in Fig. 2. The personal computer (PC) processes the read-write of the motor control card 6020 by software, and sends the position, speed, and acceleration orders into the control card. Then the control card produces a pulse sequence according to the orders of the mainframe. The number of pulse (position), frequency (speed), and rate of change in frequency (acceleration) are all controlled by the mainframe. After that, the motor driver produces multi-beat pulse signals to control the motor rotation according to the received pulse. Clockwise or anti-clockwise rotation of angle is decided by software, so as to change the relative position among the sample, the incidence, and the detector.

For suppressing the stray light and improving the measurement precision, the theory of single-reference measurement is chosen[10]. Using the single-reference measurement, the incident zenith angle of the tested sample must be identical to that of the reference. In order to get the hemisphere space scattering characteristic on the sample surface, the No. 1 motor drives the sample tilting, then the incident zenith angle is changed. Therefore, we can only revolve the No. 2 motor to compensate the change of incident zenith angle. It is supposed that the incident zenith angle is $\theta_{\rm i}$ and the azimuth angle is 0 when the turntable is in standard position, as shown in Fig. 3.

We suppose the sample rotates an angle $\Delta\varphi$ in the plane of the horizon after it has tilted an angle β in the vertical plane. $\alpha = \theta_{\rm i} - \Delta\varphi$ is the angle between the incidence and the axis z' which is achieved by rotating the No. 2 motor for $\Delta\varphi$. Here the vector of the incidence on the rotated coordinates is

$$\vec{A} = \begin{bmatrix} \sin\alpha \\ 0 \\ \cos\alpha \end{bmatrix}. \tag{1}$$

After the No. 1 motor drives the sample tilting β, the matrix which transforms the primary coordinate to the new coordinate is

$$\vec{B} = \begin{bmatrix} 1 & 0 & 0 \\ 0 & \cos\beta & -\sin\beta \\ 0 & \sin\beta & \cos\beta \end{bmatrix}. \tag{2}$$

In this coordinate system, the incidence vector becomes

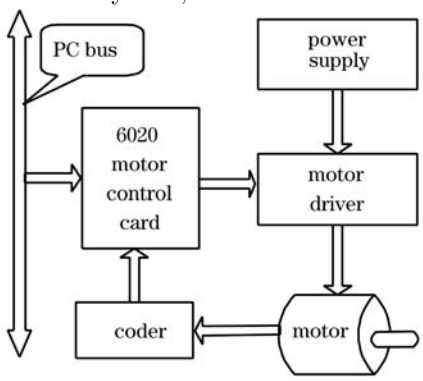

Fig. 2. Schematic of motor control.

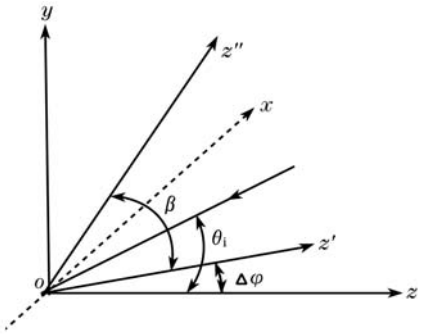

Fig. 3. Schematic diagram of incident zenith angle.

$$\vec{A}' = \begin{bmatrix} 1 & 0 & 0 \\ 0 & \cos\beta & -\sin\beta \\ 0 & \sin\beta & \cos\beta \end{bmatrix} \begin{bmatrix} \sin\alpha \\ 0 \\ \cos\alpha \end{bmatrix} = \begin{bmatrix} \sin\alpha \\ -\sin\beta\cos\alpha \\ \cos\beta\cos\alpha \end{bmatrix}. \tag{3}$$

In order to guarantee that the angle between the incidence and the new normal of the sample is the given incident zenith angle $\theta_{\rm i}$, one has

$$\cos\theta_{\rm i} = \frac{\cos\beta\cos\alpha}{\sqrt{(\sin\alpha)^2 + (-\sin\beta\cos\alpha)^2 + (\cos\beta\cos\alpha)^2}}, \tag{4}$$

$$\cos\alpha = \cos(\theta_{\rm i} - \Delta\varphi) = \frac{\cos\theta_{\rm i}}{\cos\beta}. \tag{5}$$

Therefore,

$$\Delta\varphi = \theta_{\rm i} - \arccos\left(\frac{\cos\theta_{\rm i}}{\cos\beta}\right). \tag{6}$$

From Eq. (6), we can obtain the actual $\Delta\varphi$ which the turntable needs to revolve while the incident zenith angle is still $\theta_{\rm i}$ after the sample tilts β.

Now the angle between the incidence projection on the sample plane and the new x axis is the incident azimuth angle $\varphi_{\rm i}$, thus

$$\tan\varphi_{\rm i} = \frac{-\sin\beta\cos\alpha}{\sin\alpha} = -\sin\beta(\tan\alpha)^{-1}. \tag{7}$$

Figure 4 shows the schematic diagram of scattering zenith angle on the rotated coordinates. In Fig. 4, z is the primary normal, z' is the normal after the sample rotates $\Delta\varphi$, z'' is the normal while the sample is further tilted β, $\vec{N}$ is the direction of the detector, $\theta'_{\rm S}$ is the request which is just the scattering zenith angle after transformation. Suppose the coordinates of the detector are $N = (-\sin\theta_{\rm S}, 0, \cos\theta_{\rm S})'$ on the primary coordinates. Revolving the sample first and then tilting it, the primary coordinate system has been changed twice. After revolving the sample $\Delta\varphi$ twice, the vector of the detector on the new coordinate system is

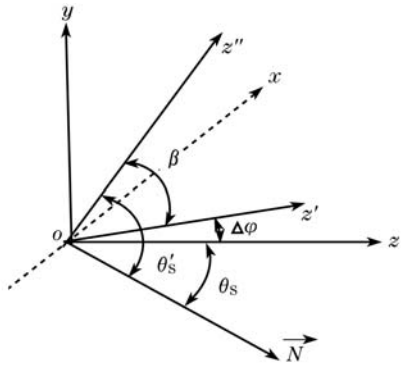

Fig. 4. Schematic diagram of scattering zenith angle.

$$\vec{N}' = \begin{bmatrix} \cos\Delta\varphi & 0 & -\sin\Delta\varphi \\ 0 & 1 & 0 \\ \sin\Delta\varphi & 0 & \cos\Delta\varphi \end{bmatrix} \begin{bmatrix} -\sin\theta_S \\ 0 \\ \cos\theta_S \end{bmatrix} = \begin{bmatrix} -\cos\Delta\varphi\sin\theta_S - \sin\Delta\varphi\cos\theta_S \\ 0 \\ -\sin\Delta\varphi\sin\theta_S + \cos\Delta\varphi\cos\theta_S \end{bmatrix}. \quad (8)$$

Then the sample is further tilted β, the coordinates of the detector become

$$\vec{N}'' = \begin{bmatrix} 1 & 0 & 0 \\ 0 & \cos\beta & -\sin\beta \\ 0 & \sin\beta & \cos\beta \end{bmatrix} \vec{N}' = \begin{bmatrix} 1 & 0 & 0 \\ 0 & \cos\beta & -\sin\beta \\ 0 & \sin\beta & \cos\beta \end{bmatrix} \begin{bmatrix} -\sin(\Delta\varphi+\theta_S) \\ 0 \\ \cos(\Delta\varphi+\theta_S) \end{bmatrix} = \begin{bmatrix} -\sin(\Delta\varphi+\theta_S) \\ -\sin\beta\cos(\Delta\varphi+\theta_S) \\ \cos\beta\cos(\Delta\varphi+\theta_S) \end{bmatrix}. \quad (9)$$

Now, the value of $\cos\theta'_S$ is

$$\cos\theta'_S = \cos\beta\cos(\Delta\varphi+\theta_S). \quad (10)$$

The value of $\tan\varphi_S$ is (φ_S is the azimuth angle of scattering light)

$$\tan\varphi_S = \frac{-\sin\beta\cos(\Delta\varphi+\theta_S)}{-\sin(\Delta\varphi+\theta_S)} = \sin\beta\left(\tan(\Delta\varphi+\theta_S)\right)^{-1}. \quad (11)$$

For spatial diffusion and non-mirror scattering measurements, the error $\varepsilon_{\mathrm{BSDF}}$ of the goniometer can be evaluated and expressed by

$$(\varepsilon_{\mathrm{BSDF}})^2 = (\varepsilon_{\mathrm{SLD}})^2 + (\varepsilon_{\theta_S})^2, \quad (12)$$

where $\varepsilon_{\mathrm{SLD}}$ is the error of the receiver view angle, which is about 0.7%; ε_{θ_S} is the error of the total scattering zenith angle, which is given by[11]

$$(\varepsilon_{\theta_S})^2 = (\varepsilon_{\theta_z})^2 + (\varepsilon_{\theta_M})^2 + (\varepsilon_{\theta_T})^2, \quad (13)$$

where ε_{θ_z} is the scattering angle error due to sample z-direction misalignment; ε_{θ_M} is the scattering angle error due to goniometer; ε_{θ_T} is the scattering angle error due to sample tilt. Based on our automative BSDF measurement setup, ε_{θ_z} is about 1°/360°, both of ε_{θ_M} and ε_{θ_T} are

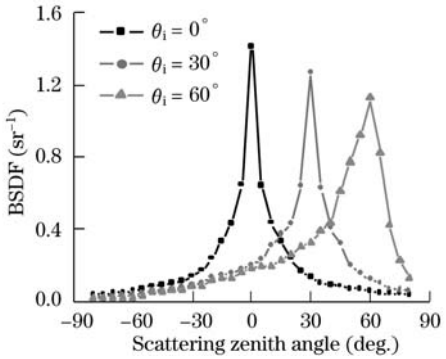

Fig. 5. Results of scattering measurement under T=25 °C.

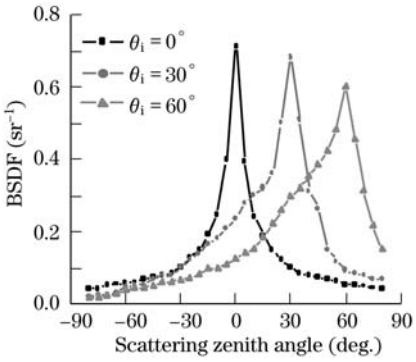

Fig. 6. Results of scattering measurement under T=380 °C.

0.072°/360° within a circle caused by the motor rotation. Then according to Eq. (13), ε_{θ_S} is about 0.28%.

Taking above results into Eq. (12), we can get

$$\varepsilon_{\mathrm{BSDF}} = \sqrt{\varepsilon_{\mathrm{SLD}}^2 + \varepsilon_{\theta_S}^2} \approx 0.75\%. \quad (14)$$

Experiments were performed with 0.6328-μm visible light under the temperatures T=25 and 380 °C, giving the bi-directional reflectance measurements on copper at $\varphi_i = 0°$ when the incident zenith angles are different. Experimental results after the angle compensation are shown in Figs. 5 and 6 respectively. As can be seen, there is a maximum value in the curve no matter what the incident angle is. In addition, the scattering angle corresponding to the maximum is close to the direction of the mirror reflection, and the peak value shifts towards right side with the increase of incident angle. Especially, the peak value reduces with the increase of the incident angle. This is because the surface is fairly gentle, the shadowing effect is not obvious, and the effective incident flux is the most important factor for the incident intensity. The corresponding mirror reflected intensity is lower and lower as a result of the incident flux reduction with the increase of incident angle.

In conclusion, based on the relative measuring method, we design the angle self-compensation setup with three degrees of freedom. The full hemispherical scattering can be almost measured. Using the theory of single-reference measurement, the expression of compensation angle is deduced. The uncertainty of the goniometer is analyzed. Experiments regarding the hemispherical reflectance measurements with visible light have been performed using the designed setup.

The authors thank Dr. Fengling Han for fruitful com-

ments. This work was supported by the National Natural Science Foundation of China (No. 50336010) and the Post Doctor Foundation of China (No. 20060390783).

References

1. Y. Cao, Z. Wu, H. Zhang, Q. Wei, and S. Wang, Acta Opt. Sin. (in Chinese) **28,** 792 (2008).
2. W. Feng, Q. Wei, S. Wang, Y. Wu, S. Liu, D. Wu, Z. Liu, and D. Wang, Acta Opt. Sin. (in Chinese) **28,** 290 (2008).
3. F. O. Bartell, E. L. Dereniak, and W. L. Wolfe, Proc. SPIE **257,** 154 (1980).
4. B. Geiger, A. Demircan, and M. von Schönermark, Proc. SPIE **4171,** 58 (2001).
5. A. T. C. Chang, D. K. Hall, and J. L. Foster, J. Remote Sensing (in Chinese) **1,** (suppl.) 11 (1997).
6. H. E. Bennett, Proc. SPIE **107,** 24 (1977).
7. G. Obein, T. Leroux, and F. Viénot, Proc. SPIE **4299,** 279 (2001).
8. D. W. Blodgett and S. C. Webb, Proc. SPIE **4257,** 448 (2001).
9. L. Zhang, Y. Yang, H. Zang, S. Hu, W. Chen, and Y. Lu, Chinese J. Lasers (in Chinese) **35,** 1001 (2008).
10. C. Qi, C. Yang, W. Li, and J. Dai, Chin. Opt. Lett. **1,** 398 (2003).
11. Z. Zhao, C. Qi, and J. Dai, Chin. Opt. Lett. **5,** 168 (2007).